Light-by-light scattering in ultraperipheral Pb-Pb collisions at energies available at the CERN Large Hadron Collider

Mariola Kłusek-Gawenda,* Piotr Lebiedowicz,† and Antoni Szczurek‡
Institute of Nuclear Physics, Polish Academy of Sciences, Radzikowskiego 152, PL-31-342 Kraków, Poland
(Received 9 February 2016; published 21 April 2016)

We calculate cross sections for diphoton production in (semi)exclusive PbPb collisions, relevant for the CERN Large Hadron Collider (LHC). The calculation is based on the equivalent photon approximation in the impact parameter space. The cross sections for the elementary $\gamma\gamma \to \gamma\gamma$ subprocess are calculated including two different mechanisms. We take into account box diagrams with leptons and quarks in the loops. In addition, we consider a vector-meson dominance (VDM-Regge) contribution with virtual intermediate hadronic (vector-like) excitations of the photons. We get measurable cross sections in PbPb collisions. This opens a possibility to study the $\gamma\gamma \to \gamma\gamma$ (quasi)elastic scattering at the LHC. We present many interesting differential distributions which could be measured by the ALICE, CMS, or ATLAS Collaborations at the LHC. We study whether a separation or identification of different components (boxes, VDM-Regge) is possible. We find that the cross section for elastic $\gamma\gamma$ scattering could be measured in the heavy-ion collisions for subprocess energies smaller than $W_{\gamma\gamma} \approx 15$–$20$ GeV.

DOI: 10.1103/PhysRevC.93.044907

I. INTRODUCTION

In classical Maxwell theory photons, waves, and wave packets do not interact. In contrast, in quantal theory they can interact via quantal fluctuations. So far only inelastic processes, i.e., production of hadrons or jets via photon-photon fusion could be measured, e.g., in e^+e^- collisions [1–4].[1]

The light-by-light scattering to the leading and next-to-leading order was discussed earlier in the literature, see [5–7], also in the context of the search for effects of new particles and interactions, e.g., see [8,9]. The cross section for elastic $\gamma\gamma \to \gamma\gamma$ scattering is so small that until recently it was beyond experimental reach. In e^+e^- collisions the energies and/or couplings of photons to electrons/positrons are rather small so that the corresponding $\gamma\gamma \to \gamma\gamma$ cross section is extremely small. A proposal to study helicity dependent $\gamma\gamma \to \gamma\gamma$ scattering in the region of MeV energies with the help of high power lasers was discussed recently, e.g., in Ref. [10].

In proton-proton collisions the subprocess energies (diphoton invariant masses) can be larger and the underlying photon-photon scattering is possible in exclusive processes [11–13]. However, at low two-photon invariant masses there is a competitive diffractive QCD mechanism through the $gg \to \gamma\gamma$ subprocess with quark boxes [14–16] which gives a much higher cross section than the photon-photon fusion [12]. The reader may find a detailed comparison of the two mechanisms in Chap. 5 of [17]. The QCD mechanism provides an explanation of experimental cross sections measured by the CDF Collaboration [18,19].

Ultraperipheral collisions (UPC) of heavy-ions provide a nice possibility to study several two-photon induced processes such as: $\gamma\gamma \to l^+l^-$,$\gamma\gamma \to \pi^+\pi^-$, $\gamma\gamma \to$ dijets, etc. (see, e.g., [20–22]). It was realized only recently that ultraperipheral heavy-ions collisions can be also a good place where photon-photon elastic scattering could be tested experimentally [11]. In Ref. [11] a first estimate of the corresponding cross section was presented.

In this paper we present a more detailed study with a more realistic approach and show several differential distributions not discussed so far. We include also a new, higher order mechanism not discussed so far in the literature.

II. $\gamma\gamma \to \gamma\gamma$ ELEMENTARY CROSS SECTION

Before presenting the nuclear cross sections let us concentrate first on elementary $\gamma\gamma \to \gamma\gamma$ scattering. The lowest order QED mechanisms with elementary particles are shown in Fig. 1. The diagram in the left panel is for lepton and quark (elementary fermion) loops, while the diagram in the right panel is for W (spin-1) boson loops. The mechanism on the left hand side dominates at lower photon-photon energies while the mechanism on the right hand side becomes dominant at higher photon-photon energies (see, e.g., [12,23]). In numerical calculations here we include box diagrams with fermions only, which will be explained in the following.

The one-loop box diagrams were calculated by using the Mathematica package FORMCALC [24] and the LOOPTOOLS library based on [25] to evaluate one-loop integrals. The complete matrix element was generated in terms of two-, three-, and four-point coefficient functions [26], internally defined photon polarization vectors, and kinematic variables (four-momenta of incoming and outgoing photons). Our result was confronted with those in [6,7,23].

*mariola.klusek@ifj.edu.pl
†piotr.lebiedowicz@ifj.edu.pl
‡Also at University of Rzeszów, PL-35-959 Rzeszów, Poland: antoni.szczurek@ifj.edu.pl

[1]Please note that here the incoming photons are virtual.

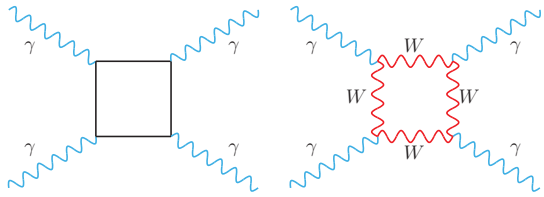

FIG. 1. Light-by-light scattering mechanisms with the lepton and quark loops (left panel) and as an example one topology of diagram for intermediate the W-boson loop (right panel).

In principle, high-order contributions, not considered so far in the context of elastic scattering, are possible too. In Ref. [7] the authors considered both the QCD and QED corrections (two-loop Feynman diagrams) to the one-loop fermionic contributions in the ultrarelativistic limit ($\hat{s},|\hat{t}|,|\hat{u}| \gg m_f^2$). The corrections are quite small numerically, showing that the leading order computations considered by us are satisfactory. In Fig. 2 (left panel) we show a process which is the same order in α_{em} but higher order in α_s. This mechanism is formally three-loop type and therefore difficult for calculation. We will not consider here the contribution of this three-loop mechanism. The exact three-loop calculation for this process is not yet available. Instead we shall consider "a similar" process shown in the right panel where both photons fluctuate into virtual vector mesons (three different light vector mesons are included). In this approach the interaction "between photons" happens when both photons are in their hadronic states.

The differential cross section for the elementary $\gamma\gamma \to \gamma\gamma$ subprocess can be calculated as

$$\frac{d\sigma_{\gamma\gamma\to\gamma\gamma}}{dt} = \frac{1}{16\pi s^2}\overline{|\mathcal{A}_{\gamma\gamma\to\gamma\gamma}|^2} \tag{2.1}$$

or

$$\frac{d\sigma_{\gamma\gamma\to\gamma\gamma}}{d\Omega} = \frac{1}{64\pi^2 s}\overline{|\mathcal{A}_{\gamma\gamma\to\gamma\gamma}|^2}\,. \tag{2.2}$$

In the most general case, including virtualities of initial photons, the amplitude can be written as $\mathcal{A} = \mathcal{A}_{TT} + \mathcal{A}_{TL} + \mathcal{A}_{LT} + \mathcal{A}_{LL}$, where $\mathcal{A}_{TL} \propto \sqrt{Q_2^2}$, $\mathcal{A}_{LT} \propto \sqrt{Q_1^2}$, $\mathcal{A}_{LL} \propto \sqrt{Q_1^2 Q_2^2}$. Since in UPC's $Q_1^2, Q_2^2 \approx 0$ (nuclear form factors kill large virtualities) the other terms can be safely neglected and $\mathcal{A} \approx \mathcal{A}_{TT}$.

The t-channel amplitude for the VDM-Regge contribution (see Fig. 2) can be written as[2]

$$\mathcal{A}_{\gamma\gamma\to\gamma\gamma}(s,t) = \sum_{i=1}^{3}\sum_{j=1}^{3} C^2_{\gamma\to V_i}\mathcal{A}_{V_iV_j\to V_iV_j}(s,t)C^2_{\gamma\to V_j} \tag{2.3}$$

$$\approx \left(\sum_{i=1}^{3} C^2_{\gamma\to V_i}\right)\mathcal{A}_{VV\to VV}(s,t)\left(\sum_{j=1}^{3} C^2_{\gamma\to V_j}\right), \tag{2.4}$$

[2]In fact the helicity amplitude can be written as $A_{\lambda_1\lambda_2\to\lambda_3\lambda_4} = \delta_{\lambda_1\lambda_3}\delta_{\lambda_2\lambda_4}A$.

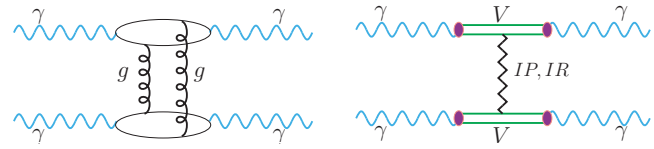

FIG. 2. Other elementary $\gamma\gamma \to \gamma\gamma$ processes. The left panel represents the two-gluon exchange and the right panel is for the VDM-Regge mechanism.

where $i,j = \rho,\omega,\phi$. The $\gamma \to V$ transition constants are taken from [27] [see Chap. 5, Eq. (1.11)]. For simplicity, we have assumed an above-universal interaction between different vector mesons:

$$\mathcal{A}_{V_iV_j\to V_iV_j}(s,t) = \mathcal{A}_{VV\to VV}(s,t) = \mathcal{A}(s,t)\exp\left(\frac{B}{2}t\right) \tag{2.5}$$

is parametrized in the Regge approach similar to $\gamma\gamma \to \rho^0\rho^0$ in Ref. [28]. Then

$$\mathcal{A}(s,t) \approx s\left((1+i)C_{I\!R}\left(\frac{s}{s_0}\right)^{\alpha_{I\!R}(t)-1} + iC_{I\!P}\left(\frac{s}{s_0}\right)^{\alpha_{I\!P}(t)-1}\right). \tag{2.6}$$

The Regge parameters for the VV interactions are taken as the same as for the $\pi^0\pi^0$ interaction. The latter can be obtained assuming Regge factorization [29]. The parameters for πN and NN scattering can be obtained from the analysis of the energy dependence of corresponding total cross sections. For example the parameters of the $\pi^0 p \to \pi^0 p$ interaction can be obtained by the averaging

$$\mathcal{A}_{\pi^0 p}(s,t) = \tfrac{1}{2}\left(\mathcal{A}_{\pi^+ p}(s,t) + \mathcal{A}_{\pi^- p}(s,t)\right). \tag{2.7}$$

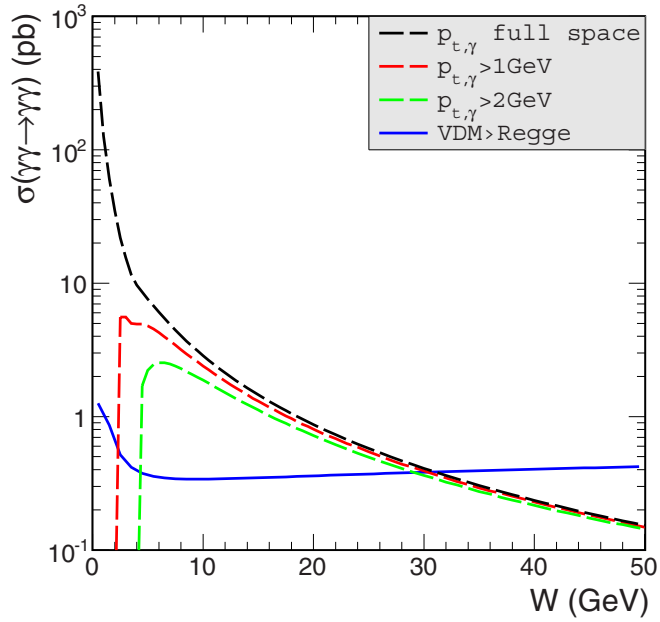

FIG. 3. Integrated $\gamma\gamma \to \gamma\gamma$ cross section as a function of the subsystem energy. The dashed lines show the contribution of boxes and the solid line represents the result of the VDM-Regge mechanism.

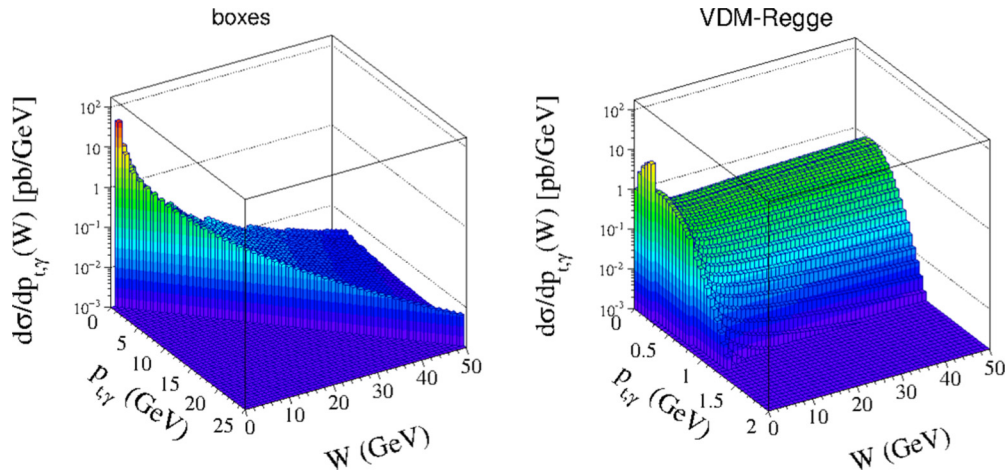

FIG. 4. Elementary cross section $d\sigma/dp_{t,\gamma}$ as a function of the subprocess energy W ($\gamma\gamma$ invariant mass in the nuclear process) and transverse momentum of one of the outgoing photons for the box (left panel) and VDM-Regge (right panel) mechanisms.

Our amplitudes here are normalized such that the optical theorem reads (for massless particles)

$$\sigma^{\rm tot}_{\pi^\pm p}(s) = \frac{1}{s}{\rm Im}\mathcal{A}_{\pi^\pm p}(s,t=0)\,. \tag{2.8}$$

The π^+p,π^-p,pp,pn total cross sections were measured and are well parametrized by the Donnachie-Landshoff parametrization [30]. Then corresponding parameters for the exchange of Pomeron and subleading Reggeons can be extracted and used in the following [29]. Some parameters ($C_{\gamma\to\rho^0}$, $C_{I\!R}$,$C_{I\!P}$) are also the same as for the VDM-Regge model for $\gamma\gamma\to\rho^0\rho^0$ [28]. The slope parameter [see Eq. (2.5)], in general a free parameter, should be similar as for the pion-pion (dipole-dipole) scattering. For a simple estimate here we take $B = 4\,{\rm GeV}^{-2}$ as in our previous paper on double ρ^0 production [28].

The elementary angle-integrated cross section for the box and VDM-Regge contributions is shown in Fig. 3 as a function of the photon-photon subsystem energy. Lepton and quark amplitudes interfere in the cross section for the box contribution. For instance in the $4 < W < 50$ GeV region, neglecting interference effects, the lepton contribution to the box cross section is by a factor 5 bigger than the quark contribution. Interference effects are, however, large and cannot be neglected. At energies $W > 30$ GeV the VDM-Regge cross section becomes larger than that for the box diagrams. Can this be seen or identified in heavy ion lead-lead collisions at the CERN Large Hadron Collider (LHC) including experimental cuts? We will try to answer this question in this paper.

For completeness in Fig. 4 we show also the differential cross section for the box (left panel) and the VDM-Regge (right panel) components as a function of subsystem energy and photon transverse momentum. The distribution for the box mechanism (left panel) has a characteristic enhancement for $p_{t,\gamma} \approx W/2$ which is due to Jacobian variable transformation from finite $d\sigma/dz$ distribution at $z = \cos\theta = 0$, where θ is the photon scattering angle in the center-of-mass system. One can observe a fast fall-off of the differential cross section with photon transverse momenta for the VDM-Regge mechanism (right panel). Imposing lower $p_{t,\gamma}$ cuts in experiments would

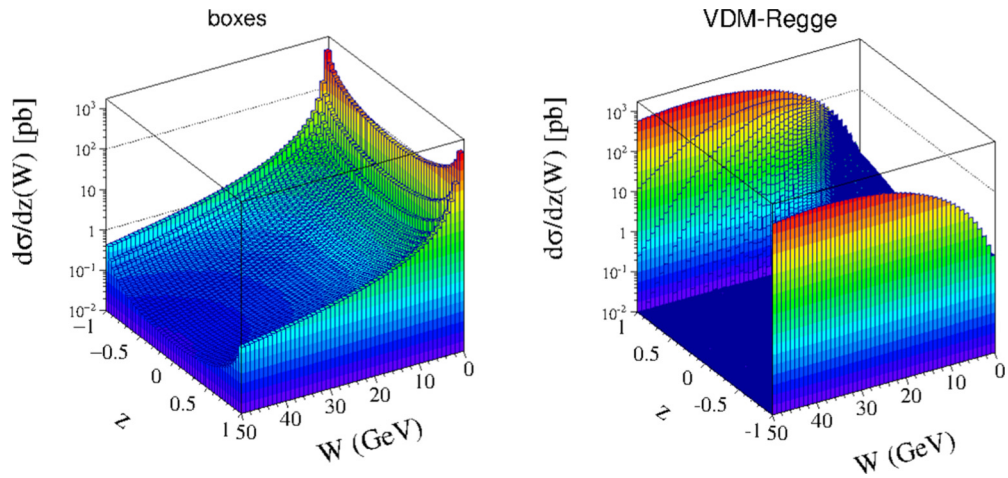

FIG. 5. Elementary cross section $d\sigma/dz$ as a function of the subprocess energy W ($\gamma\gamma$ invariant mass in the nuclear process) and $z = \cos\theta$ for the box (left panel) and VDM-Regge (right panel) mechanisms.

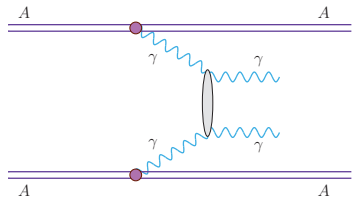

FIG. 6. $AA \to AA\gamma\gamma$ in ultrarelativistic UPC of heavy ions.

therefore almost completely kill the VDM-Regge contribution. We expect that compared to our soft VDM-Regge component the two-gluon exchange component (see the left panel of Fig. 2) should have larger wings/tails at larger transverse momenta. This may be a bit of an academic problem but may be interesting by itself.

Figure 5 presents two-dimensional distribution of the elementary $\gamma\gamma \to \gamma\gamma$ cross section as a function of the cosine of a photon scattering angle and energy. The left panel shows distribution for the box mechanism and the right panel is for the VDM-Regge mechanism. For both cases, the largest cross section occurs at $z \approx \pm 1$.

Now we shall proceed to nuclear calculations where the elementary cross sections discussed above are main ingredients of the approach.

III. DIPHOTON PRODUCTION IN UPC OF HEAVY IONS

The general situation for $AA \to AA\gamma\gamma$ is sketched in Fig. 6. Here we follow our earlier approach applied already to different reactions [28,31–36]. In our equivalent photon approximation (EPA) in the impact parameter space, the total (phase space integrated) cross section is expressed through the five-fold integral (for more details see, e.g., [31])

$$\sigma_{A_1A_2\to A_1A_2\gamma\gamma}(\sqrt{s_{A_1A_2}}) = \int \sigma_{\gamma\gamma\to\gamma\gamma}(W_{\gamma\gamma}) N(\omega_1,\mathbf{b_1}) \times N(\omega_2,\mathbf{b_2}) S^2_{abs}(\mathbf{b}) 2\pi b\,\mathrm{d}b\,\mathrm{d}\bar{b}_x\,\mathrm{d}\bar{b}_y \times \frac{W_{\gamma\gamma}}{2}\mathrm{d}W_{\gamma\gamma}\,\mathrm{d}Y_{\gamma\gamma}\,, \tag{3.1}$$

where $N(\omega_i,\mathbf{b_i})$ are photon fluxes[3] and

$$Y_{\gamma\gamma} = \tfrac{1}{2}(y_{\gamma_1} + y_{\gamma_2}) \tag{3.2}$$

is a rapidity of the outgoing $\gamma\gamma$ system. $\mathbf{b_1}$ and $\mathbf{b_2}$ are impact parameters of the photon-photon collision point with respect to parent nuclei 1 and 2, respectively, and $\mathbf{b} = \mathbf{b_1} - \mathbf{b_2}$ is a standard impact parameter for the A_1A_2 collision. The quantities $\bar{b}_x, \bar{b}_y$ are expressed through $\bar{b}_x = (b_{1x} + b_{2x})/2$ and $\bar{b}_y = (b_{1y} + b_{2y})/2$. Then

$$\mathbf{b_1} = \left[\bar{b}_x + \frac{b}{2}, \bar{b}_y\right], \qquad \mathbf{b_2} = \left[\bar{b}_x - \frac{b}{2}, \bar{b}_y\right]. \tag{3.3}$$

The invariant mass of the $\gamma\gamma$ system is defined as

$$W_{\gamma\gamma} = \sqrt{4\omega_1\omega_2}\,, \tag{3.4}$$

where $\omega_{1/2} = W_{\gamma\gamma}/2\exp(\pm Y_{\gamma\gamma})$.

Equation (3.1) allows to calculate total cross section, distributions in the impact parameter ($b = b_m$), invariant mass of the diphoton system ($W_{\gamma\gamma} = M_{\gamma\gamma}$), or rapidity of the pair ($Y_{\gamma\gamma}$) of these particles. $S^2_{abs}(b)$ is a geometrical factor which takes into account the survival probability of nuclei as a function of impact parameter. To a reasonable approximation it can be approximated as

$$S^2_{abs}(b) = \theta(b - (R_A + R_B))\,. \tag{3.5}$$

The photon flux $[N(\omega,b)]$ is expressed through a nuclear form factor. In our calculations we shall use two different types of form factor. The first one, called here the realistic form factor, is a Fourier transform of the charge distribution in nuclei and the second one is a monopole form factor $[F_{mon} = \Lambda^2/(\Lambda^2 + q^2)$, where $\Lambda = 88$ MeV to describe the charge radius of ^{208}Pb]. We shall show results using mainly the realistic form factor. More details can be found, e.g., in [31].

If one wishes to impose some cuts on produced particles (photons) which come from experimental requirements or to

[3]Nuclear charge form factors are main ingredients of the photon flux [31].

TABLE I. Integrated cross sections in nb for exclusive diphoton production processes with both photons measured for $\sqrt{s_{NN}} = 5.5$ TeV (LHC). The calculations were performed within impact-parameter EPA. The values of the total cross sections are shown for different cuts on kinematic variables for both outgoing photons.

	boxes		VDM-Regge	
cuts	$F_{\text{realistic}}$	F_{monopole}	$F_{\text{realistic}}$	F_{monopole}
$W_{\gamma\gamma} > 5$ GeV	306	349	31	36
$W_{\gamma\gamma} > 5$ GeV, $p_{t,\gamma} > 2$ GeV	159	182	7×10^{-9}	8×10^{-9}
$E_\gamma > 3$ GeV	16 692	18 400	17	18
$E_\gamma > 5$ GeV	4 800	5 450	9	11
$E_\gamma > 3$ GeV, $\lvert y_\gamma\rvert < 2.5$	183[a]	210	8×10^{-2}	9×10^{-2}
$E_\gamma > 5$ GeV, $\lvert y_\gamma\rvert < 2.5$	54	61	4×10^{-4}	7×10^{-4}
$p_{t,\gamma} > 0.9$ GeV, $\lvert y_\gamma\rvert < 0.7$ (ALICE cuts)	107			
$p_{t,\gamma} > 5.5$ GeV, $\lvert y_\gamma\rvert < 2.5$ (CMS cuts)	10			

[a]Using the Glauber model $[S^2_{abs}(b) = \exp(-\sigma^{tot}_{NN}\int \mathrm{d}^2 s T_A(b-s)T_A(s))]$ instead of the approximation which is given in Eq. (3.5) we get 177 nb.

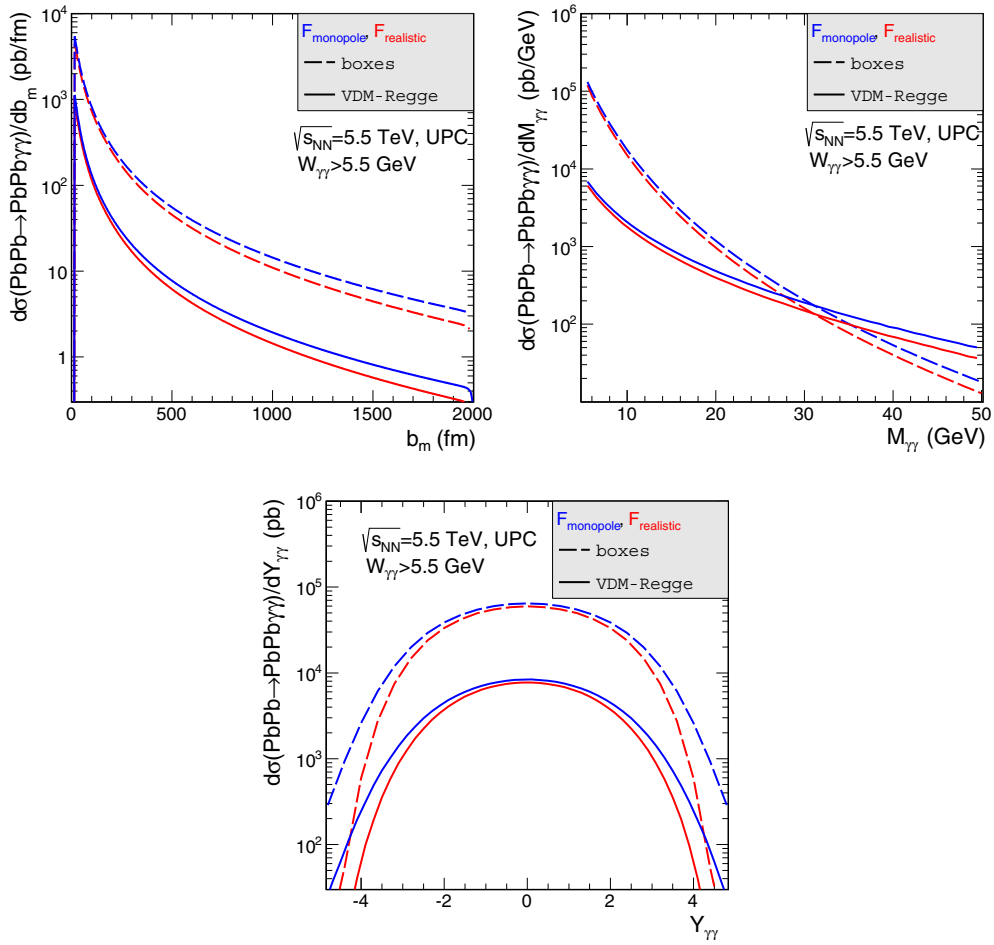

FIG. 7. Predictions for the PbPb $\to$ PbPb$\gamma\gamma$ reaction in UPC of heavy ions. Differential nuclear cross section as a function of impact parameter, $\gamma\gamma$ invariant mass, and rapidity of photon pairs at $\sqrt{s_{NN}} = 5.5$ TeV and with extra cut on $W_{\gamma\gamma} > 5.5$ GeV. The distributions with realistic charge density are depicted by the red (lower) lines and the distributions which are calculated using the monopole form factor are shown by the blue (upper) lines. The dashed lines show the results for the case when only box contributions (fermion loops) are included. The solid lines show the results for the VDM-Regge mechanism.

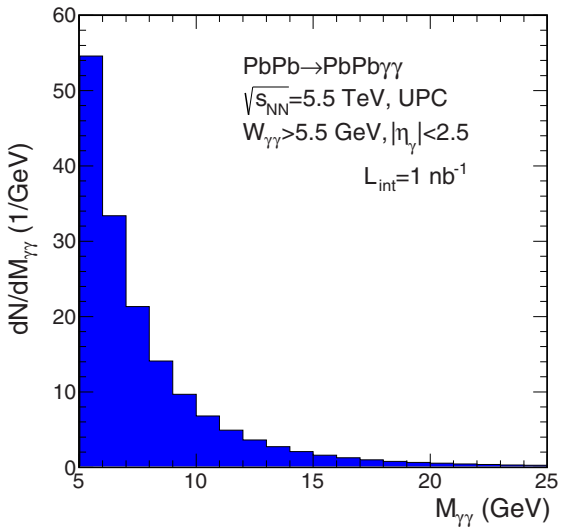

FIG. 8. Distribution of the expected number of counts in 1 GeV bins for cuts specified in the figure legend. This figure should be compared with a similar figure in [11].

have distribution in some helpful and interesting kinematical variables of individual particles (here photons), more complicated calculations are required. Then we have to introduce into the integration an additional dimension related to angular distribution for the subprocess (e.g., $z = \cos\theta$ or $p_{t,\gamma}$). Then we define kinematical variables of photons in the $\gamma\gamma$ center-of-mass system (denoted here by an asterisk):

$$E^*_{\gamma_i} = p^*_{\gamma_i} = \frac{W_{\gamma\gamma}}{2}\,, \tag{3.6}$$

$$z = \cos\theta^* = \sqrt{1 - \left(\frac{p_{t,\gamma}}{p^*_{\gamma_i}}\right)^2}\,, \tag{3.7}$$

$$p^*_{z,\gamma_i} = \pm z p^*_{\gamma_i}\,, \tag{3.8}$$

$$y^*_{\gamma_i} = \frac{1}{2}\ln\frac{E^*_{\gamma_i} + p^*_{z,\gamma_i}}{E^*_{\gamma_i} - p^*_{z,\gamma_i}}, \tag{3.9}$$

and in overall AA center-of-mass system:

$$y_{\gamma_i} = Y_{\gamma\gamma} + y^*_{\gamma_i} , \tag{3.10}$$

$$p_{z,\gamma_i} = p_{t,\gamma} \sinh(y_{\gamma_i}) , \tag{3.11}$$

$$E_{\gamma_i} = \sqrt{p^2_{z,\gamma_i} + p^2_{t,\gamma}} , \tag{3.12}$$

where $i = 1,2$ means first or second outgoing photon, respectively.

IV. RESULTS

To illustrate the general situation, in Table I we have collected integrated cross sections corresponding to different kinematical cuts. Here we show results for the two (boxes, VDM-Regge) mechanisms separately[4] for very different kinematical situations. In all cases considered, the cross section obtained with the monopole form factor is more than 10% bigger than that obtained with the realistic form factor (Fourier transform of the nucleus charge distribution). In the first row we show results for cuts from Ref. [11]. We get a similar cross section than that found in [11].[5] In this case the VDM-Regge contribution not considered in earlier calculations constitutes about 10% of the dominant box contribution. Already the cut on the transverse momentum of photons as large as $p_{t,\gamma} > 2$ GeV completely kills the VDM-Regge contribution which is very forward/backward peaked. For the box contribution the effect is much smaller. The cut on photon-photon energies is not necessary. If we impose only cuts on the energy of photons in the overall (nucleus-nucleus) center-of-mass system (laboratory frame) the box-contribution is much larger, of the order of μb. However, restricting to the rapidity coverage of the main detector diminishes the cross sections considerably, especially for the VDM-Regge contribution. The explanation will become clear when discussing differential distributions below.

In Fig. 7 we show results which can be obtained by calculating the five-fold integral [see Eq. (3.1)]. In this calculation we have imposed only a lower cut (5.5 GeV) on the photon-photon energy (or diphoton invariant mass) to get rid of the resonance region which may be more complicated. Each of the distributions (in $b_m, M_{\gamma\gamma}, Y_{\gamma\gamma}$ for boxes and VDM-Regge) is shown for the case of the realistic charge density and monopole form factor in nuclear calculations. The difference between the results becomes larger with larger values of the kinematical variables. The cross section obtained with the monopole form factor is larger for each case. The distribution in impact parameter, purely theoretical (cannot be checked experimentally), quickly drops with growing impact parameter. The distribution in invariant mass seems rather interesting. While at low invariant masses the box contribution wins, at invariant masses $M_{\gamma\gamma} > 30$ GeV the VDM-Regge contribution is bigger. Can we thus observe experimentally the VDM-Regge contribution? The matter is a bit more complicated as will be explained below. The distribution in diphoton rapidity may wrongly suggest that all photons are produced at midrapidities. We shall discuss this in detail in the following.

Can something be measured with the help of the LHC detectors? In Fig. 8 we show numbers of counts in the 1 GeV intervals expected for the assumed integrated luminosity of 1 nb^{-1}, where in addition to the lower cut on photon-photon energy we have imposed cuts on (pseudo)rapidities of both photons. It looks one can measure invariant mass distribution up to $M_{\gamma\gamma} \approx 15$ GeV.

Now we wish to show some selected results with essentially no cuts except for a minimal cut to assure that the VDM-Regge

[4]By doing so we neglect possible interference effects between the two mechanisms.

[5]Their old calculation (see Phys. Rev. Lett.) gives $\sigma = 35 \pm 7$ nb and their new calculation (see erratum to the first version) gives $\sigma = 370 \pm 70$ nb.

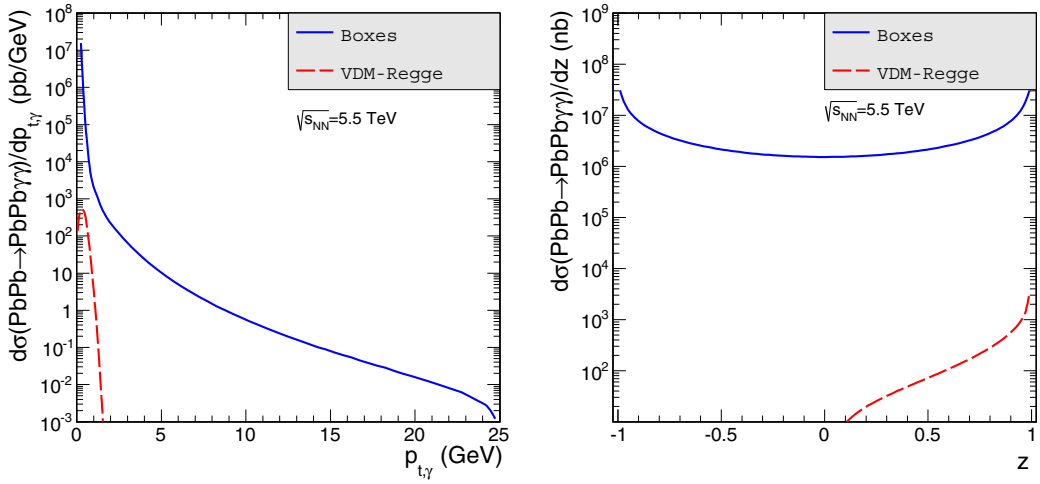

FIG. 9. Results for the PbPb $\to$ PbPb$\gamma\gamma$ reaction in UPC of heavy ions. Differential nuclear cross section as a function of photon transverse momentum $p_{t,\gamma}$ and cosine of the angle between outgoing photons $z = \cos\theta^*$ at $\sqrt{s_{NN}} = 5.5$ TeV with a minimal cut on $M_{\gamma\gamma} > 1$ GeV for the VDM-Regge mechanism only. The solid lines show the results for the case when only box contributions (fermionic loops) are included. The dashed lines show the results for the VDM-Regge approach only.

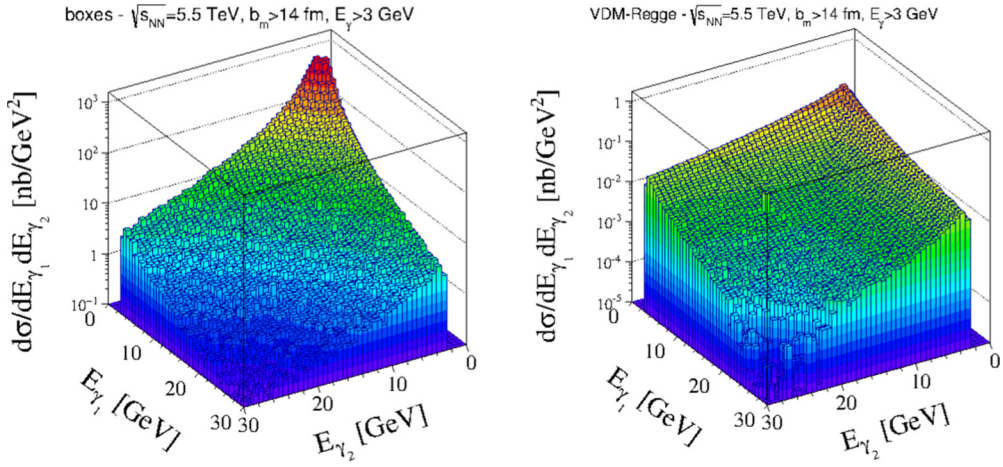

FIG. 10. Two-dimensional distribution in energies of the two photons in the laboratory frame for box (left panel) and VDM-Regge (right panel) contributions.

model applies. Figure 9 shows differential cross section as a function of photon transverse momentum $p_{t,\gamma}$ (left panel) and the cosine of the angle between outgoing photons $z = \cos\theta^*$ (right panel). The calculations are done at the LHC energy $\sqrt{s_{NN}} = 5.5$ TeV. Here we impose no cuts on kinematical variables for the box contribution and VDM-Regge mechanism except the $M_{\gamma\gamma} > 1$ GeV condition. We know that the VDM-Regge mechanism does not apply below this value. One can observe that the nuclear $d\sigma/dp_{t,\gamma}$ distribution falls very quickly for both mechanisms and is very narrow for the VDM-Regge contribution. The distribution in z (right panel) shows that without cuts on kinematical variables the maximal cross section occurs at $z \approx \pm 1$. We show only one-half of the z distribution for the VDM-Regge approach, because we include only the contribution from the t channel in our calculation. Contribution from the u channel should have similar shape as the t channel distribution but for the second half of the z distribution and would be symmetric to the t channel contribution around $z = 0$. We see that already for $W_{\gamma\gamma} = M_{\gamma\gamma} > 1$ GeV it is not necessary to symmetrize the t and u diagrams.

The cuts on photon-photon energies are, in principle, not necessary. What are in fact energies of photons in the laboratory frame of reference? In Fig. 10 we show the distribution of energies of both photons, separately for the two mechanisms: boxes (left panel) and VDM-Regge (right panel). In this calculation we do not impose cuts on $W_{\gamma\gamma}$ but only minimal cuts required by experiments on energies of individual photons ($E_\gamma > 3$ GeV) in the laboratory frame. Slightly different distributions are obtained for boxes and VDM-Regge mechanisms. For the box mechanism we can observe a pronounced maximum when both energies are small. For both mechanisms the maximum of the cross section occurs for rather asymmetric configurations: $E_1 \gg E_2$ or $E_1 \ll E_2$.

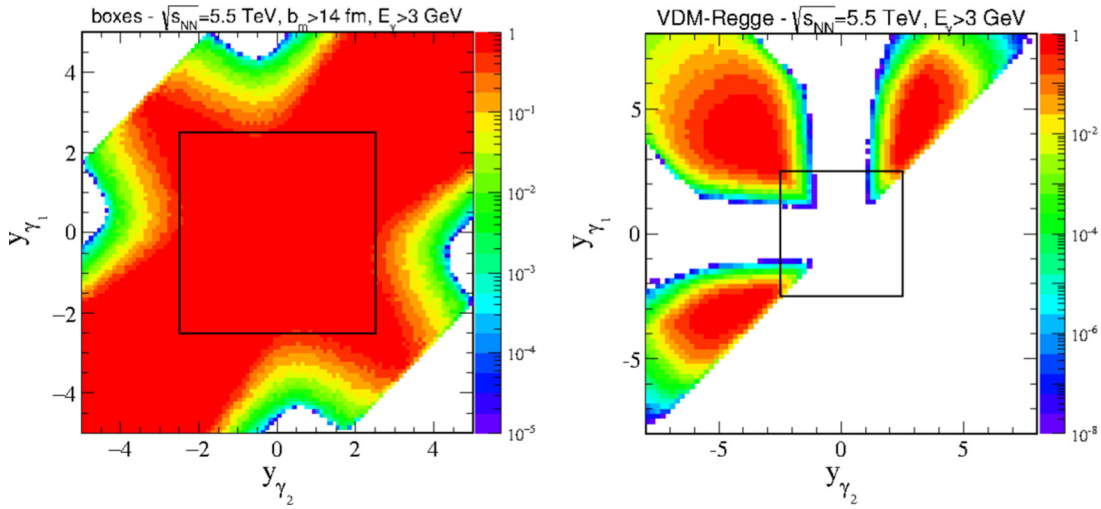

FIG. 11. Contour representation of two-dimensional ($d\sigma/dy_{\gamma_1} dy_{\gamma_2}$ in nb) distribution in rapidities of the two photons in the laboratory frame for box (left panel) and VDM-Regge (right panel) contributions with shown experimental rapidity coverage of the main ATLAS or CMS detectors. Only one-half of the $(y_{\gamma_1}, y_{\gamma_2})$ space is shown for the VDM-Regge contribution. The second half can be obtained from the symmetry around the $y_{\gamma_1} = y_{\gamma_2}$ line.

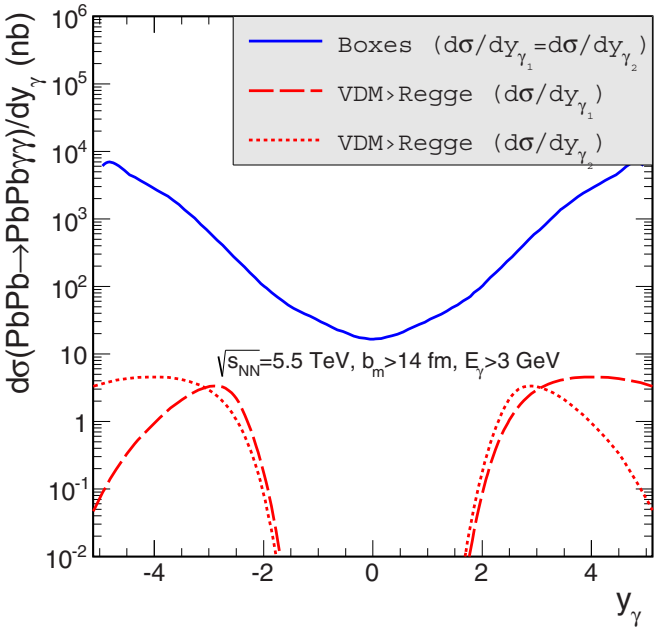

FIG. 12. Projection on rapidity of one of the photons. The cuts here are the same as in Fig. 11. For the VDM contribution, the dashed and dotted lines are projections on the y_{γ_1} and y_{γ_2} axes, respectively.

In Fig. 11 we show two-dimensional distributions in photon rapidities in the contour representation with the experimental limitations $[y_{\gamma_1}, y_{\gamma_2} \in (-2.5, 2.5)]$ of the main detectors. These distributions are very different for the box and VDM-Regge contributions. In both cases the influence of the imposed cuts is significant. In the case of the VDM-Regge contribution we observe noncontinuous behavior (dip in the cross section, better visible in Fig. 12 where we show projections on both axes) which is caused by the strong transverse momentum dependence of the elementary cross section (see Fig. 4) which causes some regions in the two-dimensional space are almost not populated. The white (empty) areas in the upper-left and lower-right corners for the box case are caused by a finite number of points in a grid at $z \approx \pm 1$. For the case of the VDM-Regge contribution we show distribution for only one-half of the $(y_{\gamma_1}, y_{\gamma_2})$ space. Clearly the VDM-Regge contribution does not fit to the main detector and extends towards large rapidities. Could photons originating from this mechanism be measured with the help of so-called zero-degree calorimeters (ZDCs) associated with the ATLAS or CMS main detectors? In the case of the VDM-Regge contribution (right panel) we show a much broader range of rapidity than for the box component (left panel). We discover that maxima of the cross section associated with the VDM-Regge mechanism are at $|y_{\gamma_1}|, |y_{\gamma_2}| \approx 5$. Unfortunately this is below the limitations of the ZDCs $|\eta| > 8.3$ for the ATLAS [37] or 8.5 for the CMS collaborations [38].

V. CONCLUSIONS

We have performed detailed feasibility studies of elastic photon-photon scattering in ultraperipheral heavy ion collisions at the LHC. The calculation was performed in an equivalent photon approximation in the impact parameter space. This method allows to remove those cases when nuclei collide and therefore break apart. Such cases are difficult in interpretation and were omitted here.

The cross section for elementary photon-photon scattering has been calculated including box diagrams with elementary standard model particles as well as a new component called here "VDM-Regge" for brevity. This soft component is based on the idea of hadronic fluctuation of the photon(s). The photons interact when they are in their hadronic (virtual vector meson) states. The standard soft Regge phenomenological type of interaction is used for the hadron-hadron interaction. The VDM-Regge mechanism gives, in general, a much smaller cross section but for $W_{\gamma\gamma} > 30$ GeV starts to dominate over the box contributions, at least in the full phase space.

Several EPA distributions in the standard kinematical variables were calculated. The results for the box component were compared to results of earlier calculations in the literature. We have made an estimate of the counting rate with expected integrated luminosity. We expect some counts $(N > 1)$ for $W_{\gamma\gamma} = M_{\gamma\gamma} < 15$–$20$ GeV.

We have performed a detailed calculation including also distributions of individual outgoing photons by extending the standard EPA. We have made an estimation of the integrated cross section for different experimental situations relevant for the ALICE or CMS experiments as well as shown several differential distributions. We observe a significant influence on experimentally required cuts. We have studied whether the VDM-Regge component, not discussed so far, could be identified experimentally and have shown that it will probably be very difficult.

We have found that, very different than for the box contribution, the VDM-Regge contribution reaches a maximum of the cross section when $(y_{\gamma_1} \approx 5, y_{\gamma_2} \approx -5)$ or $(y_{\gamma_1} \approx -5, y_{\gamma_2} \approx 5)$. This is a rather difficult region which cannot be studied, e.g., with ZDC's installed at the LHC.

So far we have studied only the diphoton continuum. The resonance mechanism could also be included in the future. In the present studies we have concentrated on the signal. Future studies should also include an estimation of the background. The dominant background may be expected from $AA \to AAe^+e^-$ when both electrons are misidentified as photons.

ACKNOWLEDGMENTS

We are indebted to D. d'Enterria and G. da Silveira for informing us about an erratum to their paper on a similar subject. The discussion on the ALICE acceptance for photons with Adam Matyja is acknowledged. This work was partially supported by the Polish National Science Centre Grant No. DEC-2014/15/B/ST2/02528 (OPUS) as well as by the Centre for Innovation and Transfer of Natural Sciences and Engineering Knowledge in Rzeszów. A part of the calculations within this analysis was carried out with the help of the cloud computer system [Cracow Cloud One (cc1.ifj.edu.pl)] of the Institute of Nuclear Physics Polish Academy of Sciences.

[1] D. Buskulic *et al.* (ALEPH Collaboration), An experimental study of $\gamma\gamma \to$ hadrons at LEP, Phys. Lett. B **313**, 509 (1993).

[2] K. Muramatsu *et al.* (TOPAZ Collaboration), Measurement of the photon structure function $F_2(\gamma)$ and jet production at TRISTAN, Phys. Lett. B **332**, 477 (1994).

[3] K. Ackerstaff *et al.* (OPAL Collaboration), Inclusive jet production in photon-photon collisions at $\sqrt{s} = 130$-GeV and 136-GeV, Z. Phys. C **73**, 433 (1997).

[4] R. Barate *et al.* (ALEPH Collaboration), Study of fermion pair production in e^+e^- collisions at 130-GeV to 183-GeV, Eur. Phys. J. C **12**, 183 (2000).

[5] M. Bohm and R. Schuster, Scattering of light by light in the electroweak standard model, Z. Phys. C **63**, 219 (1994).

[6] G. Jikia and A. Tkabladze, Photon-photon scattering at the photon linear collider, Phys. Lett. B **323**, 453 (1994).

[7] Z. Bern, A. De Freitas, L. J. Dixon, A. Ghinculov, and H. L. Wong, QCD and QED corrections to light-by-light scattering, J. High Energy Phys. 11 (2001) 031.

[8] G. J. Gounaris, P. I. Porfyriadis, and F. M. Renard, Light by light scattering at high-energy: A Tool to reveal new particles, Phys. Lett. B **452**, 76 (1999); Erratum: Light by light scattering at high energy: a tool to reveal new particles [Phys. Lett. B 452 (1999) 7682], **513**, 431(E) (2001).

[9] G. J. Gounaris, P. I. Porfyriadis, and F. M. Renard, The $\gamma\gamma \to \gamma\gamma$ process in the standard and SUSY models at high-energies, Eur. Phys. J. C **9**, 673 (1999).

[10] K. Homma, K. Matsuura, and K. Nakajima, Testing helicity dependent $\gamma\gamma \to \gamma\gamma$ scattering in the region of MeV, Prog. Theor. Exp. Phys. **2016**, 013C01 (2016).

[11] D. d'Enterria and G. G. da Silveira, Observing light-by-light scattering at the Large Hadron Collider, Phys. Rev. Lett. **111**, 080405 (2013); Erratum: Observing Light-by-Light Scattering at the Large Hadron Collider [Phys. Rev. Lett. 111, 080405 (2013)], **116**, 129901(E) (2016).

[12] P. Lebiedowicz, R. Pasechnik, and A. Szczurek, Search for technipions in exclusive production of diphotons with large invariant masses at the LHC, Nucl. Phys. B **881**, 288 (2014).

[13] S. Fichet, G. von Gersdorff, O. Kepka, B. Lenzi, C. Royon, and M. Saimpert, Probing new physics in diphoton production with proton tagging at the Large Hadron Collider, Phys. Rev. D **89**, 114004 (2014).

[14] V. A. Khoze, A. D. Martin, M. G. Ryskin, and W. J. Stirling, Diffractive gamma-gamma production at hadron colliders, Eur. Phys. J. C **38**, 475 (2005).

[15] P. Lebiedowicz, R. Pasechnik, and A. Szczurek, QCD diffractive mechanism of exclusive W^+W^- pair production at high energies, Nucl. Phys. B **867**, 61 (2013).

[16] L. A. Harland-Lang, V. A. Khoze, M. G. Ryskin, and W. J. Stirling, Central exclusive production within the Durham model: a review, Int. J. Mod. Phys. A **29**, 1430031 (2014).

[17] P. Lebiedowicz, Exclusive reactions with light mesons: From low to high energies. http://www.ifj.edu.pl/msd/rozprawy_dr/rozpr_Lebiedowicz.pdf, 2014.

[18] T. Aaltonen *et al.* (CDF Collaboration), Search for Exclusive $\gamma\gamma$ Production in Hadron-Hadron Collisions, Phys. Rev. Lett. **99**, 242002 (2007).

[19] T. Aaltonen *et al.* (CDF Collaboration), Observation of Exclusive $\gamma\gamma$ production in $p\bar{p}$ collisions at $\sqrt{s} = 1.96$ TeV, Phys. Rev. Lett. **108**, 081801 (2012).

[20] G. Baur, K. Hencken, D. Trautmann, S. Sadovsky, and Y. Kharlov, Coherent $\gamma\gamma$ and $\gamma - A$ interactions in very peripheral collisions at relativistic ion colliders, Phys. Rep. **364**, 359 (2002).

[21] C. A. Bertulani, S. R. Klein, and J. Nystrand, Physics of ultraperipheral nuclear collisions, Annu. Rev. Nucl. Part. Sci. **55**, 271 (2005).

[22] A. J. Baltz, The physics of ultraperipheral collisions at the LHC, Phys. Rep. **458**, 1 (2008).

[23] D. Bardin, L. Kalinovskaya, and E. Uglov, Standard model light-by-light scattering in SANC: analytic and numeric evaluation, Phys. Atom. Nucl. **73**, 1878 (2010).

[24] T. Hahn and M. Perez-Victoria, Automatized one loop calculations in four-dimensions and D-dimensions, Comput. Phys. Commun. **118**, 153 (1999).

[25] G. J. van Oldenborgh and J. A. M. Vermaseren, New algorithms for one loop integrals, Z. Phys. C **46**, 425 (1990).

[26] G. Passarino and M. Veltman, One loop corrections for e^+e^- annihilation into $\mu^+\mu^-$ in the Weinberg model, Nucl. Phys. B **160**, 151 (1979).

[27] B. L. Ioffe, V. A. Khoze, and L. N. Lipatov, *Hard Processes*, Vol. 1: Phenomenology, Quark Parton Model (North-Holland, Amsterdam, 1985).

[28] M. Kłusek, W. Schäfer, and A. Szczurek, Exclusive production of $\rho^0\rho^0$ pairs in gamma gamma collisions at RHIC, Phys. Lett. B **674**, 92 (2009).

[29] A. Szczurek, N. N. Nikolaev, and J. Speth, From soft to hard regime in elastic pion pion scattering above resonances, Phys. Rev. C **66**, 055206 (2002).

[30] A. Donnachie and P. V. Landshoff, Total cross-sections, Phys. Lett. B **296**, 227 (1992).

[31] M. Kłusek-Gawenda and A. Szczurek, Exclusive muon-pair productions in ultrarelativistic heavy-ion collisions—realistic nucleus charge form factor and differential distributions, Phys. Rev. C **82**, 014904 (2010).

[32] M. Kłusek-Gawenda, A. Szczurek, M. V. T. Machado, and V. G. Serbo, Double-photon exclusive processes with heavy quark–heavy antiquark pairs in high-energy Pb-Pb collisions at LHC, Phys. Rev. C **83**, 024903 (2011).

[33] M. Kłusek-Gawenda and A. Szczurek, Exclusive production of large invariant mass pion pairs in ultraperipheral ultrarelativistic heavy ion collisions, Phys. Lett. B **700**, 322 (2011).

[34] S. Baranov, A. Cisek, M. Kłusek-Gawenda, W. Schäfer, and A. Szczurek, The $\gamma\gamma \to J/\psi J/\psi$ reaction and the $J/\psi J/\psi$ pair production in exclusive ultraperipheral ultrarelativistic heavy ion collisions, Eur. Phys. J. C **73**, 2335 (2013).

[35] M. Kłusek-Gawenda and A. Szczurek, $\pi^+\pi^-$ and $\pi^0\pi^0$ pair production in photon-photon and in ultraperipheral ultrarelativistic heavy ion collisions, Phys. Rev. C **87**, 054908 (2013).

[36] M. Kłusek-Gawenda and A. Szczurek, Double-scattering mechanism in the exclusive $AA \to AA\rho^0\rho^0$ reaction in ultrarelativistic collisions, Phys. Rev. C **89**, 024912 (2014).

[37] P. Jenni, M. Nessi, and M. Nordberg, Zero Degree Calorimeters for ATLAS, Report No. LHCC-I-016, CERN-LHCC-2007-001.

[38] O. A. Grachov *et al.* (CMS Collaboration), Performance of the combined zero degree calorimeter for CMS, J. Phys. Conf. Ser. **160**, 012059 (2009).